# Spectral and localization properties of the Dirichlet wave guide with two concentric Neumann discs

**H. Najar**

Départemente de Mathématiques, ISMAI, Kairouan, Bd Assed Ibn Elfourat, 3100 Kairouan Tunisia

E-mail: `hatem.najar@ipeim.rnu.tn`

**O. Olendski**[1,2,3]

[1]Department of Physics, Jackson State University, 1400 Lynch St., Jackson, MS 39217 USA
[2]Atomic and Molecular Engineering Laboratory, Belarusian State University, Skarina Av. 4, Minsk 220050 Belarus
‡[3]King Abdullah Institute for Nanotechnology, King Saud University, P.O. Box 2455, Riyadh 11451 Saudi Arabia

E-mail: `oolendski@ksu.edu.sa`

**Abstract.** Bound states of the Hamiltonian describing a quantum particle living on three dimensional straight strip of width $d$ are investigated. We impose the Neumann boundary condition on the two concentric windows of the radii $a$ and $b$ located on the opposite walls and the Dirichlet boundary condition on the remaining part of the boundary of the strip. We prove that such a system exhibits discrete eigenvalues below the essential spectrum for any $a, b > 0$. When $a$ and $b$ tend to the infinity, the asymptotic of the eigenvalue is derived. A comparative analysis with the one-window case reveals that due to the additional possibility of the regulating energy spectrum the anticrossing structure builds up as a function of the inner radius with its sharpness increasing for the larger outer radius. Mathematical and physical interpretation of the obtained results is presented; namely, it is derived that the anticrossings are accompanied by the drastic changes of the wave function localization. Parallels are drawn to the other structures exhibiting similar phenomena; in particular, it is proved that, contrary to the two-dimensional geometry, at the critical Neumann radii true bound states exist.

**AMS Classification:** 81Q10 (47B80, 81Q15)

**Keywords:** Quantum Waveguide, Shrödinger operator, bound states, Dirichlet Laplcians.

‡ Present address

## 1. Introduction

The task of finding eigenenergies $E_n$ and corresponding eigenfunctions $f_n(\mathbf{r})$, $n = 1, 2, ...$ of the Laplacian in the two- (2D) and three-dimensional (3D) domain $\Omega$ with mixed Dirichlet

$$f_n(\mathbf{r})|_{\partial\Omega_D} = 0 \tag{1}$$

and Neumann

$$\mathbf{n}\boldsymbol{\nabla} f_n(\mathbf{r})|_{\partial\Omega_N} = 0 \tag{2}$$

boundary conditions on its confining surface (for 3D) or line (for 2D) $\partial\Omega = \partial\Omega_D \cup \partial\Omega_N$ ($\mathbf{n}$ is a unit normal vector to $\partial\Omega$) [1–8] are commonly referred to as Zaremba problem [9]. One class of such systems that recently received a lot of attention from mathematicians and physicists are 2D and 3D straight and bent quantum wave guides [10–32]. In particular, the conditions for the existence of the bound states and resonances in such classically unbound system were considered for the miscellaneous permutations of the Dirichlet and Neumann domains [14, 19, 25]. Bound states lying below the essential spectrum of the corresponding straight part were predicted to exist for the curved 2D channel if its inner and outer interfaces support the Dirichlet and Neumann requirements, respectively, and not for the opposite configuration [16, 18, 21]. This was an extension of the previous theoretical studies of the existence of the bound states for the pure Dirichlet bent wave guide [33, 34] that were confirmed experimentally [35]. Magnetic field influence on the Dirichlet-Neumann structures was analyzed too [25, 27]. Also, for the 2D straight Dirichlet wave guide the existence of the bound state below the essential spectrum was predicted when the Neumann window is placed on its confining surface [10, 12]. The number of the bound states increases with the window length $L$ and their energies are monotonically decreasing functions of $L$ [17]. Recently, this result was extended to the case of the 3D spatial Dirichlet duct with circular Neumann disc [30] for which a proof of the bound state existence was confirmed, the number of discrete eigenvalues as a function of the disc radius $a$ was evaluated and their asymptotics for the large $a$ was given.

In the present research, we discuss the case of the two concentric Neumann windows with, in general, different radii $a$ and $b$ on the opposite walls of the 3D straight wave guide. A comparative analysis with the one Neumann disk reveals that the two-window geometry offers more possibilities for the varying spectral and localization properties by the additional channel of changing the second disc radius. Namely, its variation leads to the formation of the anticrossing structure of the energy spectrum as a function of smaller radius $b$ when the almost flat parts of the energy $b$-dependence are alternated by their sharp drops down to the lower level pushing it to occupy the next lying below neighbouring state, etc. Transitions get sharper and the gaps between the anticrossing states decrease with increasing the outer radius $a$. These avoided crossings are accompanied by the drastic changes of the localization of the wave function.

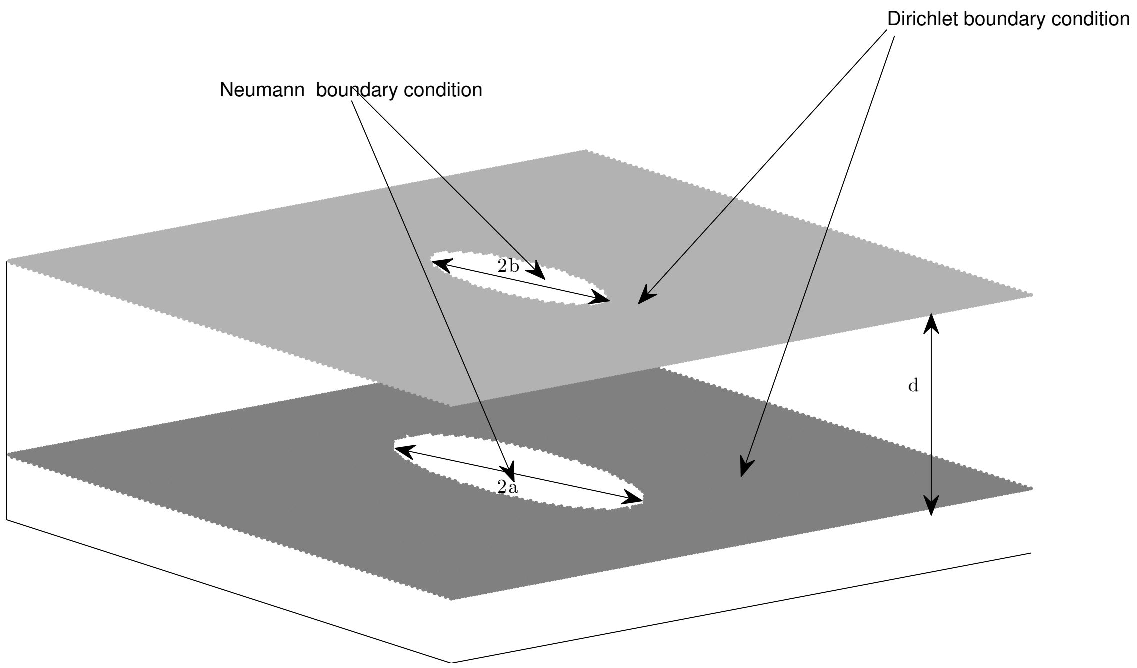


**Figure 1.** Dirichlet wave guide with two concentric Neumann disc windows on the opposite walls with (in general) different radii $a$ and $b$.

The rest of the paper is organized as follows. In section 2, we define the model and recall some known results. In section 3, we present the main result of this investigation followed by a discussion. Section 4 is devoted for numerical experiments, and concluding remarks are collected in section 5.

## 2. Model and Formulation

The system we are going to study is given in figure 1. We consider a Schrödinger particle with mass $m_p$ whose motion is confined to a pair of parallel planes separated by the width $d$. For simplicity, we assume that they are placed at $z = 0$ and $z = d$. We shall denote this configuration space by $\Omega$

$$\Omega = \mathbb{R}^2 \times [0, d].$$

Let $\gamma_0(a)$ be a disc of radius $a$ with its center at $(0, 0, 0)$ and $\gamma_d(b)$ be a disc of radius $b$ centered at $(0, 0, d)$, where

$$\gamma_\cdot(z) = \{(x, y, \cdot) \in \mathbb{R}^3;\ x^2 + y^2 \leq z^2\}. \tag{3}$$

Without loss of generality we assume that $0 \leq b \leq a$. We set $\Gamma = \partial\Omega \diagdown (\gamma_0(a) \cup \gamma_d(b))$. We consider Dirichlet boundary condition on $\Gamma$ and Neumann boundary condition in $\gamma_0(a)$ and $\gamma_d(b)$ what means that $\partial\Omega_D$ and $\partial\Omega_N$ from (1) and (2) take the following form: $\partial\Omega_D \equiv \Gamma$, $\partial\Omega_N \equiv \gamma_0(a) \cup \gamma_d(b)$.

### 2.1. The Hamiltonian

Let us define the self-adjoint operator on $L^2(\Omega)$ corresponding to the particle Hamiltonian $\hat{H}$. This is done by means of the quadratic forms. Namely, let $q_0$ be the quadratic form

$$q_0(f,g) = \int_\Omega \overline{\nabla f} \cdot \nabla g d\mathbf{r}, \text{ with domain } \mathcal{Q}(q_0) = \{f \in H^1(\Omega);\ f\lceil \partial\Omega_D = 0\}, \quad (4)$$

where $H^1(\Omega) = \{f \in L^2(\Omega) | \nabla f \in L^2(\Omega)\}$ is the standard Sobolev space and we denote by $f\lceil\partial\Omega_D$ the trace of the function $f$ on $\partial\Omega_D$. It follows that $q_0$ is a densely defined, symmetric, positive and closed quadratic form. We denote the unique self-adjoint operator associated with $q_0$ by $\hat{H}$ and its domain by $D(\Omega)$. It is the Hamiltonian describing our system. From [36] (page 276), we infer that the domain $D(\Omega)$ of $\hat{H}$ is

$$D(\Omega) = \left\{ f \in H^1(\Omega);\ -\Delta f \in L^2(\Omega), f\lceil\partial\Omega_D = 0, \frac{\partial f}{\partial z}\lceil\partial\Omega_N = 0 \right\}$$

and

$$\hat{H} f = -\Delta f, \quad \forall f \in D(\Omega),$$

where we have set $\hbar^2/(2m_p) \equiv 1$.

### 2.2. Some known facts

Let us start this subsection by recalling that in the particular case when $a = b = 0$, we get $\hat{H}^0$, the Dirichlet Laplacian, and at $a = b = +\infty$ we get $\hat{H}^\infty$, the Neumann Laplacian. Since

$$\hat{H} = (-\Delta_{\mathbb{R}^2}) \otimes I \oplus I \otimes \left(-\Delta_{[0,d]}\right), \text{on } L^2(\mathbb{R}^2) \otimes L^2([0,d]),$$

(see [36]) we get that the spectrum of $\hat{H}^0$ is $\left[\left(\frac{\pi}{d}\right)^2, +\infty\right[$ and the spectrum of $\hat{H}^\infty$ is $[0, +\infty[$. Consequently, we have

$$\left[\left(\frac{\pi}{d}\right)^2, +\infty\right[ \subset \sigma\left(\hat{H}\right) \subset [0, +\infty[.$$

This leads to a natural choice of the unit of energy as $(\pi/d)^2$ used below. In addition, if not stated otherwise, we will measure all distances in units of the wave guide width $d$, and all momenta, in units of $1/d$.

Using the property that the essential spectra are preserved under compact perturbation, we deduce that the essential spectrum of $\hat{H}$ for any finite $a$ and $b$ is

$$\sigma_{ess}\left(\hat{H}\right) = [1, +\infty[.$$

An immediate consequence is that the discrete spectrum, if it exists, lies in $[0, 1]$.

*2.3. Preliminary: Cylindrical coordinates*

Let us note that the system has a cylindrical symmetry, therefore, it is natural to consider the cylindrical coordinates system $\mathbf{r} = (r, \theta, z)$. Indeed, we have that

$$L^2(\Omega, dxdydz) = L^2(]0, +\infty[\times[0, 2\pi[\times[0, 1], rdrd\theta dz).$$

We denote by $\langle , \rangle_{\mathbf{r}}$ the scalar product in $L^2(\Omega, dxdydz) = L^2(]0, +\infty[\times[0, 2\pi[\times[0, 1], rdrd\theta dz)$ given by

$$\langle f, g\rangle_{\mathbf{r}} = \int_{]0,+\infty[\times[0,2\pi[\times[0,1]} \overline{f} g r dr d\theta dz.$$

We denote the gradient in cylindrical coordinates by $\boldsymbol{\nabla}_{\mathbf{r}}$. The Laplacian operator is written as

$$\Delta_{r,\theta,z} = \boldsymbol{\nabla}_{\mathbf{r}}^2 = \frac{1}{r}\frac{\partial}{\partial r}\left(r\frac{\partial}{\partial r}\right) + \frac{1}{r^2}\frac{\partial^2}{\partial\theta^2} + \frac{\partial^2}{\partial z^2}. \tag{5}$$

Therefore, the eigenvalue equation is given by

$$-\Delta_{r,\theta,z} f(r, \theta, z) = \pi^2 E f(r, \theta, z). \tag{6}$$

Since the operator is positive, we set $\pi^2 E = k^2$. Equation (6) is solved by separating the variables and considering the function $f$ as a product

$$f(r, \theta, z) = R(r) \cdot \Theta(\theta) \cdot Z(z). \tag{7}$$

Plugging the last expression into (6), one first separates $Z$ by putting all the $z$ dependence into one term so that $\frac{Z''}{Z}$ can only be constant taken, for convenience, as $-s^2$ with its value determined by the boundary conditions at $z = 0$ and $z = 1$. Second, we separate the term $\frac{\Theta"}{\Theta}$ which has all the $\theta$ dependence. Using the fact that the problem has an axial symmetry and the solution has to be $2\pi$ periodic and single-valued in $\theta$, we obtain that $\frac{\Theta"}{\Theta}$ should be a constant $-m^2$ for $m \in \mathbb{Z}$. Finally, we get the following equation for $R$

$$R''(r) + \frac{1}{r}R'(r) + \left(k^2 - s^2 - \frac{m^2}{r^2}\right) R(r) = 0. \tag{8}$$

We notice that equation (8) is the Bessel equation and its solutions could be expressed in terms of the Bessel functions [37, 38]. More explicit solutions could be given by considering boundary conditions; for example, for the Dirichlet requirements at the both walls one has $s_j^{DD} = (j + 1)\pi$ while for the NN situation $s_j^{NN} = j\pi$, and for the mixed case $s_j^{ND} = (j + 1/2)\pi$, $j \in \mathbb{N}$ (see Section 4 for more discussion).

## 3. The result

The main result of the present research is the following

**Theorem 3.1** *The operator $\hat{H}$ has at least one isolated eigenvalue in $[0, 1]$ for any $a$ and $b$ such that $a + b > 0$.*

*Moreover, for b big enough, if $\lambda(a,b)$ is an eigenvalue of $\hat{H}$ less then 1, then we have*

$$\lambda(a,b) \in \left(\frac{1}{a^2}, \frac{1}{b^2}\right). \tag{9}$$

**Remark 3.2** *The first claim of Theorem 3.1 is valid for more general shape of bounded surface $\mathcal{S}$ with Neumann boundary condition, not necessarily a disc; it suffices that the surface contains a disc of radius $a > 0$.*

For the more general shape $\mathcal{S}$, using discs of radii $a$ and $a'$ such that

$$\gamma_0(a) \subset \mathcal{S} \subset \gamma_0(a'), \tag{10}$$

and a comparison argument, one gets the localization of the discrete spectrum.

**Proof.** For the first claim we may mimic the argument given in [30]; indeed, as we consider the function on the form domain we construct a function $\Phi \in \mathcal{D}_0(\Omega)$ such that the functional

$$q[\Phi] = \mathcal{Q}_0[\Phi] - \pi^2 \|\Phi\|^2_{L^2(\Omega, rdrd\theta dz)} \tag{11}$$

is less then zero. Here, $\mathcal{Q}_0(f,g)$ is a quadratic form defined as

$$\mathcal{Q}_0(f,g) = \langle \boldsymbol{\nabla} f, \boldsymbol{\nabla} g\rangle_{\mathbf{r}} \tag{12}$$

with domain

$$\mathcal{D}_0(\Omega) = \left\{ f \in L^2(\Omega, rdrd\theta dz); \boldsymbol{\nabla}_{\mathbf{r}} f \in L^2(\Omega, rdrd\theta dz); f\lceil \partial\Omega_D = 0 \right\}.$$

Since the essential spectrum of $\hat{H}$ starts at 1, as $q[\Phi]$ has a negative value then the task is achieved. Following [30], let us choose the candidate function $\Phi$ in the form

$$\Phi(r,\theta,z) = \varphi(r)\chi_0^{DD}(z) \tag{13}$$

with $\chi_0^{DD}(z)$ being a ground-state transverse function:

$$\chi_0^{DD}(z) = \begin{cases} \sqrt{2}\sin(\pi z), & z \in [0,1] \\ 0, & z \notin [0,1]. \end{cases} \tag{14}$$

After substituting (13) into (11), one gets after elementary algebra:

$$q[\Phi] = 2\pi \|\varphi'\|^2_{L^2(]0,+\infty[, rdr)}. \tag{15}$$

Next, consider the interval $J := [0,c]$ with $c > a$ and a function $\varphi \in \mathcal{S}([0,+\infty[)$ such that $\varphi(r) = 1$ for $r \in J$. Let us define a family of functions $\{\varphi_\tau : \tau > 0\}$ such that

$$\varphi_\tau(r) = \begin{cases} \varphi(r), & r \in (0,c) \\ \varphi\left(c + \tau \ln(r/c)\right), & r \geq c. \end{cases} \tag{16}$$

By the change of variables in the integrand, one can show that

$$\|\varphi'_\tau\|^2_{L^2([0,+\infty[, rdr)} = \tau \int_0^\infty |\varphi'(s)|^2\, ds = \tau \|\varphi'\|^2_{L^2([0,+\infty[)}. \tag{17}$$

For any radial localization function $j(r)$ from $C_0^\infty(0,a)$ and for the arbitrary $\tau, \varepsilon > 0$ let us define

$$\Phi_{\tau,\varepsilon}(r,z) = \varphi_\tau(r)\left[\chi_0^{DD}(z) + \varepsilon j(r)^2\right]. \tag{18}$$

Since the supports of $\varphi_\tau$ and $j$ are disjoint, one gets after some math using properties of the function $\chi_0^{DD}(z)$ and equation (17):

$$\begin{aligned} q\left[\Phi_{\tau,\varepsilon}\right] &= 2\pi\tau\|\varphi'\|^2_{L^2([0,+\infty[)} - 8\pi\varepsilon\|j^2\|^2_{L^2([0,+\infty[)} \\ &+ 2\pi\varepsilon^2\left[2\|jj'\|^2_{L^2([0,+\infty[,rdr)} - \pi^2\|j^2\|^2_{L^2([0,+\infty[,rdr)}\right]. \end{aligned} \tag{19}$$

The first term in the right-hand side of (19) depends on $\tau$ only being independent of $\varepsilon$ while the second negative term linear in $\varepsilon$ for the quite small $\varepsilon$ dominates over the last quadratic term. Accordingly, choosing relevant $\tau$ and $\varepsilon$, one gets the negative $q\left[\Phi_{\tau,\varepsilon}\right]$. ■

The proof of the second claim is based on the bracketing argument. Let us split $L^2(\Omega, rdrd\theta dz)$ as follows: $L^2(\Omega, rdrd\theta dz) = L^2(\Omega^-_{a,b}, rdrd\theta dz) \oplus L^2(\Omega^+_{a,b}, rdrd\theta dz)$, with

$$\begin{aligned} \Omega^-_{a,b} &= \{(r,\theta,z) \in [0, b+(a-b)(1-z)] \times [0,2\pi[\times[0,1]\}, \\ \Omega^+_{a,b} &= \Omega\backslash\Omega^-_{a,b}. \end{aligned}$$

Therefore,

$$\hat{H}^{-,N}_{a,b} \oplus \hat{H}^{+,N}_{a,b} \leq \hat{H} \leq \hat{H}^{-,D}_{a,b} \oplus \hat{H}^{+,D}_{a,b}.$$

Here, we index by $D$ and $N$ depending on the boundary conditions considered on the surface $r = b + (a-b)(1-z)$. The min-max principle leads to

$$\sigma_{ess}\left(\hat{H}\right) = \sigma_{ess}\left(\hat{H}^{+,N}_{a,b}\right) = \sigma_{ess}\left(\hat{H}^{+,D}_{a,b}\right) = [1,+\infty[\,.$$

Hence, if $\hat{H}^{-,D}_{a,b}$ exhibits a discrete spectrum below 1, then $\hat{H}$ does as well. We mention that this is not a necessary condition. If we denote by $\lambda_j\left(\hat{H}^{-,D}_{a,b}\right), \lambda_j\left(\hat{H}^{-,N}_{a,b}\right)$ and $\lambda_j\left(\hat{H}\right)$ the $j$-th eigenvalue of $\hat{H}^{-,D}_{a,b}$, $\hat{H}^{-,N}_{a,b}$ and $\hat{H}$, respectively, then, again, the minimax principle yields the following

$$\lambda_j\left(\hat{H}^{-,N}_{a,b}\right) \leq \lambda_j\left(\hat{H}\right) \leq \lambda_j\left(\hat{H}^{-,D}_{a,b}\right) \tag{20}$$

and for $j \geq 2$

$$\lambda_{j-1}\left(\hat{H}^{-,D}_{a,b}\right) \leq \lambda_j\left(\hat{H}\right) \leq \lambda_j\left(\hat{H}^{-,D}_{a,b}\right). \tag{21}$$

As the computation of the eigenvalue of a frustum is not an easy task, let us remark that

$$\lambda_j\left(\hat{H}^{-,D}_{a,a}\right) \leq \lambda_j\left(\hat{H}^{-,D}_{a,b}\right) \leq \lambda_j\left(\hat{H}^{-,D}_{b,b}\right)$$

(the same chain of inequalities is true for the corresponding Neumann Hamiltonians $\hat{H}^{-,N}$, too). The Hamiltonian $\hat{H}^{-,D}_{b,b}$ has a sequence of eigenvalues [37, 38] given by

$$\lambda_{nml} = (n\pi)^2 + \left(\frac{x_{ml}}{b}\right)^2,$$

where $x_{ml}$ is the $l$-th positive zero of Bessel function of the order $m$ (see [37, 38]) . The condition

$$\lambda_{nml} \leq 1 \tag{22}$$

yields that $n = 0$, so we get

$$\lambda_{0ml}(b) = \left(\frac{x_{ml}}{b}\right)^2.$$

and

$$\lambda_{0m'l'}(a) = \left(\frac{x_{m'l'}}{a}\right)^2.$$

This yields that the condition (22) to be fulfilled, will depend on the value of $\left(\frac{x_{ml}}{b}\right)^2$.

We recall that $x_{ml}$ are the positive zeros of the Bessel function $J_m(x)$. So, for any eigenvalue $\lambda(a, b)$ of the Hamiltonian $\hat{H}$, there exist $m, l, m', l' \in \mathbb{N}$ such that

$$\frac{x_{ml}^2}{a^2} \leq \lambda(a, b) \leq \frac{x_{m'l'}^2}{b^2}. \tag{23}$$

When $b$ is big enough, we get the result. ■

Next statement describes the case when the new bound state just emerges from the continuum what means that its energy is equal to the Dirichlet fundamental propagation threshold. We assume that the inner radius is either fixed in the interval $0 \leq b < a$ or is equal to its outer counterpart $a$.

**Proposition 3.3** *When the radius $a$ is equal to a critical value $a_l$ at which a new bound state emerges from the continuum, equation (6) with $E = 1$ has a solution $f_l^{(0)}(r, \theta, z)$, unique to a multiplicative constant which at infinity behaves like*

$$f_l^{(0)}(r, \theta, z) = \frac{e^{im\theta}}{\sqrt{2\pi}} \left[ \frac{\sqrt{2}\sin \pi z}{r^{|m|}} + \beta_l \frac{e^{-\pi\sqrt{3}r}}{\sqrt{r}} \sin 2\pi z + \mathcal{O}\left( \frac{e^{-\pi\sqrt{8}r}}{\sqrt{r}} \right) \right], \quad r \to \infty \tag{24}$$

*with some constants $\beta_l$. Here, the two quantum numbers $n$ and $m$ are compacted into the single index $l$: $l \equiv (n, m)$.*

A proof of this statement will be given in the next section.

Note that the derived asymptotics from (24) drastically differs from its quasi-one-dimensional couterpart [10, 11, 17, 19]; namely, if, in the latter case, the state at $E = 1$ is *always* a resonance, for the 3D geometry considered in this paper this is true for the azimuthal quantum number $m = 0$ only, and for $|m| \geq 2$ one has true bound states with square integrable functions $f_l^{(0)}(\mathbf{r})$. We point out that the function of the state with $|m| = 1$ vanishes at infinity, however, it is not square integrable over the whole $r - \theta$ plane; accordingly, one can consider it as a resonance too. In other words, a behaviour of the states lying on the border between the essential and discrete spectra crucially depends on the dimensionality of the problem.

## 4. Numerical computations: mode-matching method

This section is devoted to some numerical computations. We analyse a dependence of the eigenenergies $E$ and coresponding eigenfunctions $f$ on the radii $a$ and $b$ in the whole range of their variation. We also compare the obtained results with the one-window case [30].

### *4.1. Two identical Neumann windows*

Consider first the case of the equal radii on the upper and lower walls of the duct. The eigenvalue equation (6) uses the Laplacian provided in (5). A general solution is written in equation (7). Since for our problem a cylindrical symmetry is conserved, one has $\Theta(\theta)=\frac{1}{\sqrt{2\pi}}e^{im\theta}$, with the integer $m$ being an azimuthal quantum number. A total solution can be written:

for one Neumann window:

$$f_<(r,\theta,z)=\frac{1}{\sqrt{2\pi}}e^{im\theta}\sum_{j=0}^{\infty}B_j^{|m|}J_{|m|}\left(\pi\sqrt{E-(j+1/2)^2}r\right)\chi_j^{ND}(z),\ r\leq a \tag{25$a$}$$

$$f_>(r,\theta,z)=\frac{1}{\sqrt{2\pi}}e^{im\theta}\sum_{j=0}^{\infty}A_j^{|m|}K_{|m|}\left(\pi\sqrt{(j+1)^2-E}r\right)\chi_j^{DD}(z),\quad r\geq a \tag{25$b$}$$

for the two identical concentric Neumann windows of the radius $a$ on the opposite walls:

$$f_<(r,\theta,z)=\frac{1}{\sqrt{2\pi}}e^{im\theta}\sum_{j=0}^{\infty}B_j^{|m|}J_{|m|}\left(\pi\sqrt{E-j^2}r\right)\chi_j^{NN}(z),\ r\leq a \tag{26}$$

and for $r\geq a$ it coincides with (25$b$). Here, $J_m(r)$ is Bessel function of the first kind with $K_m(r)$ being its modified counterpart of the second kind [37, 38], coefficients $A_j^{|m|}$ and $B_j^{|m|}$ present a relative contribution of the corresponding component into the total wave function, and the orthonormalized functions $\chi_j^{DD}(z)$, $\chi_j^{ND}(z)$ and $\chi_j^{NN}(z)$ describing a transverse motion in the Dirichlet-Dirichlet, Dirichlet-Neumann and Neumann-Neumann strips, respectively, read:

$$\chi_j^{DD}(z)=\sqrt{2}\sin(j+1)\pi z \tag{27$a$}$$

$$\chi_j^{ND}(z)=\sqrt{2}\cos(j+1/2)\pi z \tag{27$b$}$$

$$\chi_j^{NN}(z)=\begin{cases}1,\ j=0\\ \sqrt{2}\cos j\pi z,\ j\neq 0.\end{cases} \tag{27$c$}$$

Their corresponding eigenvalues are, respectively, $E_j^{DD}=(j+1)^2$, $E_j^{ND}=(j+1/2)^2$ and $E_j^{NN}=j^2$. Note that for $j\neq 0$ the Bessel functions $J_{|m|}\left(\pi\sqrt{E-(j+1/2)^2}r\right)$ in (25$a$) and $J_{|m|}\left(\pi\sqrt{E-j^2}r\right)$ in (26) transform into their modified counterparts $I_{|m|}\left(\pi\sqrt{(j+1/2)^2-E}r\right)$ and $I_{|m|}\left(\pi\sqrt{j^2-E}r\right)$ [37, 38], respectively. Functions $I_{|m|}\left(\pi\sqrt{(j+1)^2-E}r\right)$ diverging at infinity are not included into the outer solutions, equation (25$b$), in order to guarantee the finiteness of the wave function for the arbitrarily large $r$. For the same reason, another Bessel function of the first kind $Y_{|m|}\left(\pi\sqrt{E-(j+1/2)^2}r\right)$ diverging at the origin [37, 38] is not a part of solutions in equations (25$a$) and (26).

Physically, the emergence of the bound state for at least one nonzero radius is due to the fact that the introduction of one or two Neumann windows mixes longitudinal and transverse motions in the wave guide what results in the splitting off of the unbound level from the lowest subband down below the fundamental propagation threshold and its corresponding transformation into the localized state with square-integrable wave function vanishing at infinity. Mathematically, this mixing is reflected in the fact that the summation index $j$ in equations (25) and (26) enters each component of both transverse $Z(z)$ as well as radial $R(r)$ parts of the wave function binding them together. Note that this binding is different inside and outside the disc. In a sense, a Neumann perturbation of the Dirichlet duct presents a shelter where the Schrödinger particle can dwell with its momentum smaller than the cutoff momentum of the fundamental propagation threshold. Similar to the bend in curved Dirichlet wave guide [39], one can draw parallels with the creation by the obstacle of an attractive quantum well that binds the particle; namely, the wave can still be propagating inside the circle but vanishing outside: as equations ($25a$) and (26) demonstrate, there is one propagating along the radial direction component [the term with $j=0$ when the difference $E-(j+1/2)^2$ (for one window) or $E-j^2$ (for the two discs) is positive] while outside the discs the wave function possesses exponentially vanishing contributions only.

Matching function $f$ and its radial derivative at $r=a$, one gets (we consider the case of one Neumann disc; two discs situation is treated in the very same way):

$$\sum_{j=0}^{\infty} B_j^{|m|} J_{|m|}\left(\pi\sqrt{E-(j+1/2)^2}a\right)\chi_j^{ND}(z)$$
$$=\sum_{j=0}^{\infty} A_j^{|m|} K_{|m|}\left(\pi\sqrt{(j+1)^2-E}a\right)\chi_j^{DD}(z) \qquad (28a)$$
$$\sum_{j=0}^{\infty} B_j^{|m|}\sqrt{E-(j+1/2)^2}J'_{|m|}\left(\pi\sqrt{E-(j+1/2)^2}a\right)\chi_j^{ND}(z)$$
$$=\sum_{j=0}^{\infty} A_j^{|m|}\sqrt{(j+1)^2-E}K'_{|m|}\left(\pi\sqrt{(j+1)^2-E}a\right)\chi_j^{DD}(z) \qquad (28b)$$

where the prime denotes a derivative of the Bessel function with respect to its argument. Multiplying each part of the system of equations (28) by $\chi_{j'}^{DD}(z)$, $j'=0,1,\ldots$, we arrive at:

$$A_{j'}^{|m|}=\sum_{j=0}^{\infty}\frac{J_{|m|}\left(\pi\sqrt{E-(j+1/2)^2}a\right)}{K_{|m|}\left(\pi\sqrt{(j'+1)^2-E}a\right)}P_{jj'}^{(1)}B_j^{|m|} \qquad (29a)$$

$$A_{j'}^{|m|}=\sum_{j=0}^{\infty}\sqrt{\frac{E-(j+1/2)^2}{(j'+1)^2-E}}\frac{J'_{|m|}\left(\pi\sqrt{E-(j+1/2)^2}a\right)}{K'_{|m|}\left(\pi\sqrt{(j'+1)^2-E}a\right)}P_{jj'}^{(1)}B_j^{|m|} \qquad (29b)$$

where the infinite square matrix $\mathbf{P}^{(1)}$ describing the coupling between different modes of the DD and ND channels has the following elements:

$$P_{jj'}^{(1)} = \int_0^1 \chi_j^{DD}(z)\chi_{j'}^{ND}(z)dz = \frac{2}{\pi}\frac{j+1}{(j+1)^2-(j'+1/2)^2}. \tag{30}$$

From system (29) one immediately has:

$$\sum_{j'=0}^{\infty} Q_{jj'}B_{j'}^{|m|} = 0 \tag{31}$$

with the following matrix elements of the infinite square matrix $\mathbf{Q}$:

$$\begin{aligned} Q_{jj'} = & \left[\sqrt{\frac{E-(j'+1/2)^2}{(j+1)^2-E}}\frac{J'_{|m|}\left(\pi\sqrt{E-(j'+1/2)^2}a\right)}{K'_{|m|}\left(\pi\sqrt{(j+1)^2-E}a\right)}\right. \\ & \left. - \frac{J_{|m|}\left(\pi\sqrt{E-(j'+1/2)^2}a\right)}{K_{|m|}\left(\pi\sqrt{(j+1)^2-E}a\right)}\right] P_{jj'}^{(1)}. \end{aligned} \tag{32}$$

Nontrivial solution of the system (31) exists only when the determinant of the matrix $\mathbf{Q}$ is an identical zero:

$$\det ||\mathbf{Q}|| = 0. \tag{33}$$

This is an equation for determining bound-state energies $E$ for different radii $a$. For the case of the two equal windows the corresponding matrix $\mathbf{P}^{(2)}$ that substitutes $\mathbf{P}^{(1)}$ in (29) and (32) is the quantitative measure of the coupling between the different modes of the DD and NN wave guides:

$$\begin{aligned} P_{jj'}^{(2)} &= \int_0^1 \chi_j^{DD}(z)\chi_{j'}^{NN}(z)dz \\ &= \begin{cases} \frac{2}{\pi}\left[(-1)^{j+j'}+1\right]\frac{j+1}{(j+1)^2-j'^2}, & j'\neq 0, j'\neq j+1 \\ 0, & j'\neq 0, j'=j+1 \\ \frac{\sqrt{2}}{\pi(j+1)}\left[(-1)^j+1\right], & j'=0 \end{cases} \end{aligned} \tag{34}$$

From (31) the coefficients $B_j^{|m|}$ can be determined and, next, from equations (29) the values of $A_j^{|m|}$ are calculated too. Normalization condition

$$\int_0^{2\pi} d\theta \int_0^1 dz \int_0^{\infty} drr\left|f\left(r,\theta,z\right)\right|^2 = 1 \tag{35}$$

allows one to fully construct the function $f$. Note that radial integrals in (35) with the function $f$ given by equations (25) and (26) are calculated analytically [40, 41] in terms of the Bessel functions themself.

Fig. 2 depicts bound-state energies as a function of the normalized radius $a$. Both configurations show a lot of similarities. As discussed in [30] for one and earlier in this paper for the two identical Neumann windows, at least one bound state exists for the

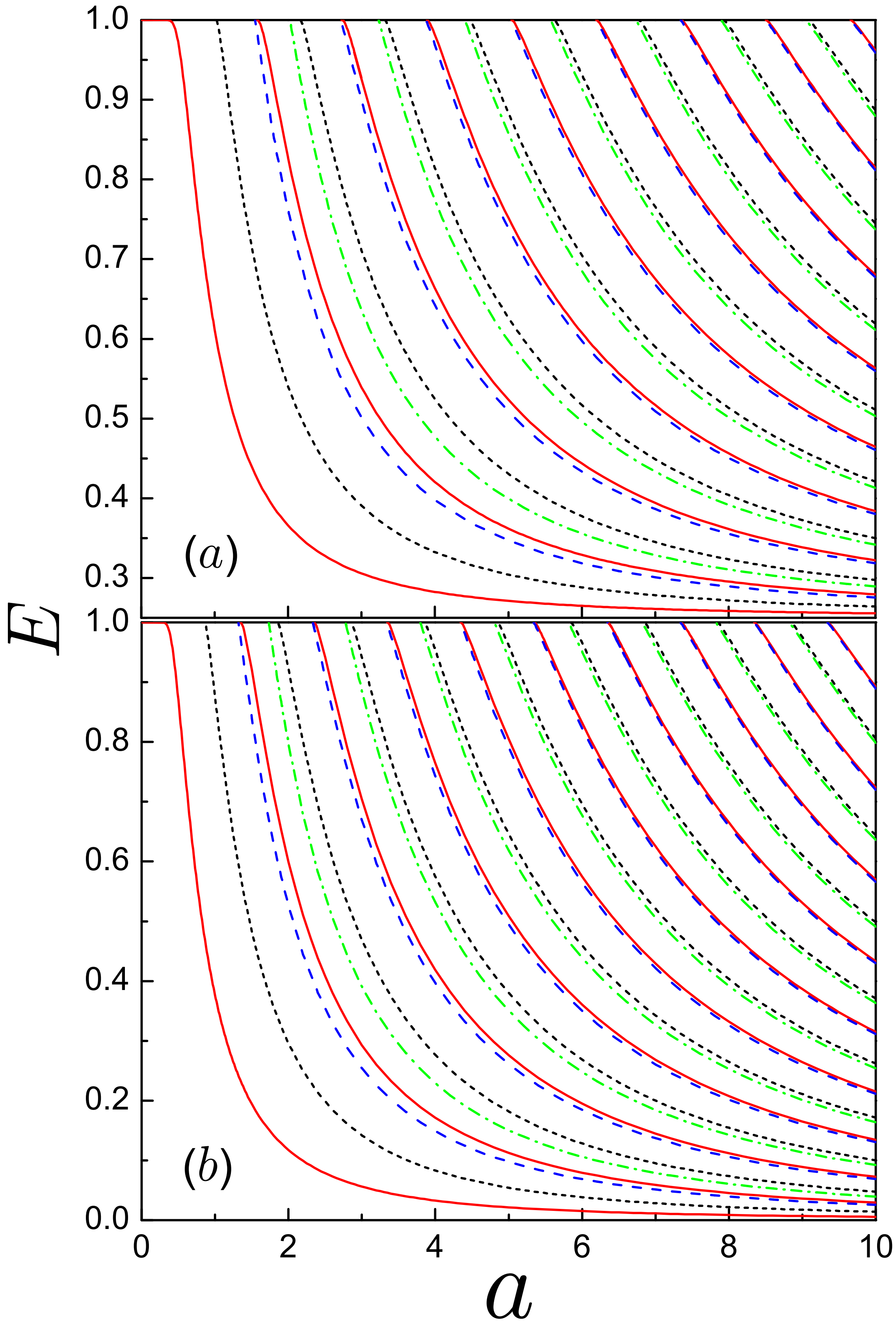


**Figure 2.** Bound-state energies $E$ as a function of the radius $a$ for (a) one Neumann window and (b) two concentric Neumann discs on the opposite sides of the wave guide where solid lines are for the states with the azimuthal quantum number $m = 0$, dotted lines - for the states with $|m| = 1$, dashed lines - for $|m| = 2$, and dash-dotted curves - for $|m| = 3$. Note different energy scales in panels (a) and (b).

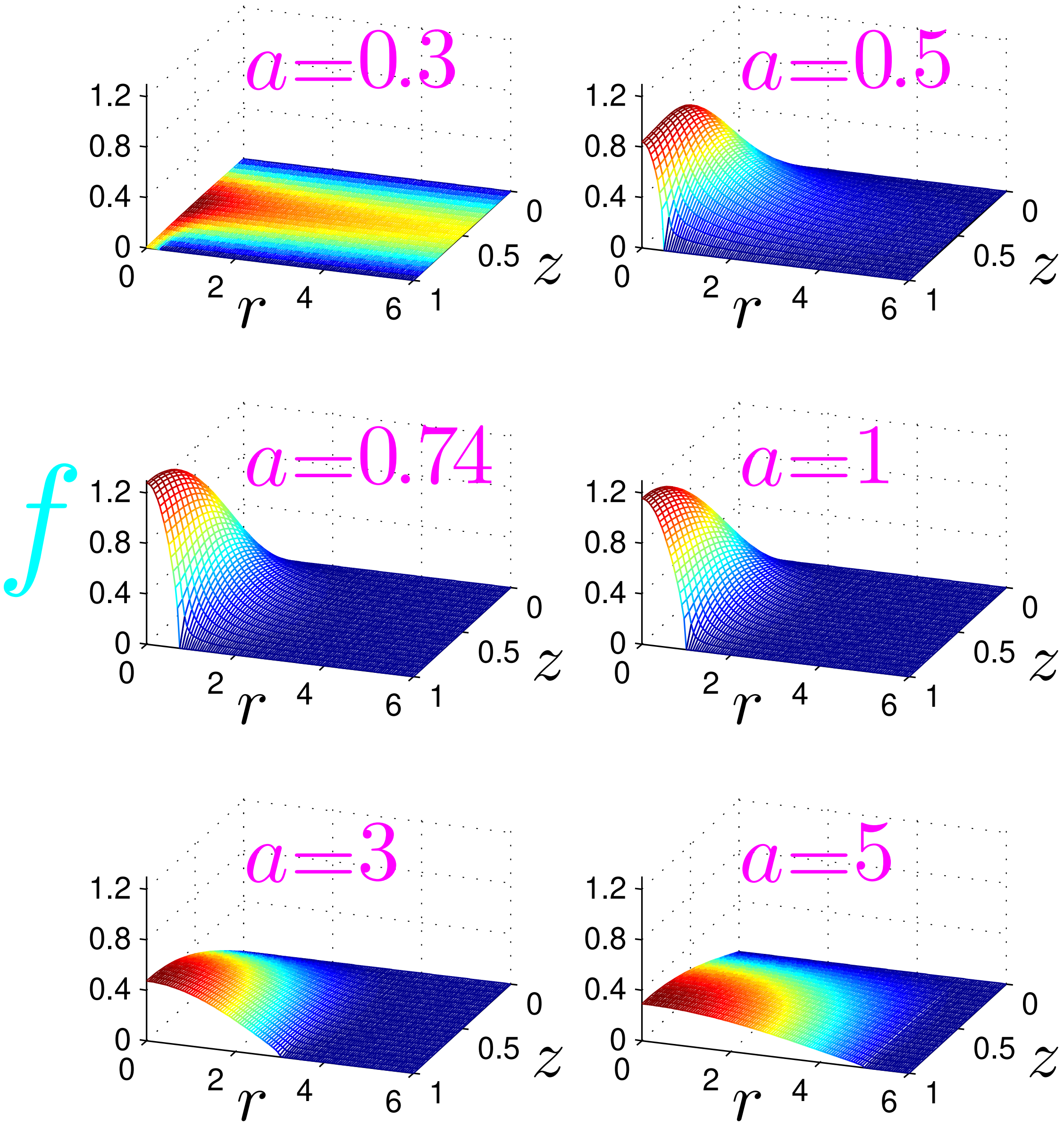


**Figure 3.** Ground bound-state wave function $f$ in terms of $r$ and $z$ for one Neumann window and several values of the radius $a$.

arbitrarily small radius $a$: in both cases this is the state with the azimuthal quantum number $m = 0$. For quite small radii its energy lies very close to the fundamental propagation threshold of the uniform Dirichlet wave guide $E_0^{DD} = 1$. Further growth of $a$ forces the bound-state energy to decrease, and at large radii it tends from above to the fundamental propagation threshold of the Neumann-Dirichlet $E_0^{ND} = 1/4$ (for one window, ref. [30]) or the uniform Neumann $E_0^{NN} = 0$ (for two windows, see above) channels. Second bound state possesses quantum number $|m| = 1$ and emerges from the continuum at $a \sim 1.027$ for one window and $a \sim 0.866$ for the two Neumann discs. This difference is not surprising since the two Neumann regions present a stronger perturbation to the particle motion in the uniform Dirichlet wave guide as compared to the one window; accordingly, in the former case the second bound state is formed at the smaller radius. This is true for all other states (but the first one) as well; for example, the third bound state with $|m| = 2$ emerges for the one disc at $a \sim 1.549$ and for the two Neumann windows - at $a \sim 1.319$. As our results show, in both cases the next bound level is another state with azimuthal quantum number $m = 0$ preceding in this way its counterpart with $|m| = 3$. Similar to the ground state, energies of the higher lying levels decrease when the radius increases with the difference between them diminishing what means the increase of the corresponding density of states (number of states per unit energy) $\mathcal{N}(E)$ until at $a = \infty$ one arrives at the continuous spectrum of the ND (one window) or NN (two windows) channel with the diverging density $\mathcal{N}(E)$.

Figures 3 and 4 depict the lowest bound-state wave function $f(r, z)$ for one and two windows, respectively, at several Neumann radii $a$. Since the lowest level possesses azimuthal quantum number $m = 0$, its wave function is $\theta$-independent. It is seen that for the small radii, say, $a = 0.3$ in figures 3 and 4, the wave function is almost flat spreading far away from the Neumann area. This can be easily understood by means of the mentioned above analogy with the quantum well [42]; namely, for the small radius $a$ the effective positive potential created by the disc, only barely binds the particle with its wave function relatively slowly vanishing at infinity. Increasing Neumann radius strengthens the attractiveness of the well; accordingly, as the panels for $a = 0.4$ (figure 4) and $a = 0.5$ (figure 3) exhibit, the function $f$ is stronger localized inside the disc with the magnitude of its maximum growing. In both configurations the maximum is achieved at the centre of the disc, $r = 0$. As our calculations show, for one window this extremum reaches it maximal value of $f_{max} \sim 1.28$ at $a \sim 0.74$ and for the two discs - at $a \sim 0.56$ with $f_{max} \sim 1.12$ (see corresponding panels in figures 3 and 4). Subsequent increase of the Neumann area makes the potential well wider and wider with the wave function $f$ being almost uniformly distributed inside it. Its radial slope diminishes, as a transition from the situation with $a = 1$ to the one with $a = 3$ and, next, to $a = 5$ in figures 3 and 4 vividly demonstrates. Such a behaviour can be easily explained implementing again the potential well model [42]. Introduction of the one Neumann disc breaks the wave guide symmetry with respect to the plane $z = 1/2$. This is reflected in the corresponding asymmetry of the wave function which inside the disc, for the fixed radius $r < a$, reaches the maximum at $z = 0$ and continuously decreases to zero at $z = 1$. On the contrary, second identical Neumann window restores this symmetry with the function $f$ reflecting it in figure 4.

It was already mentioned in the Introduction that bound states are characterized by the two quantum numbers: principal $n$ and azimuthal $m$. To exemplify this, we plot in figure 5 functions $f' \equiv \exp(-im\theta)f$ for the fixed radius $a = 3$ and several quantum numbers $(n, m)$ for both configurations of the boundary conditions. In addition to the discussed above features, one can notice that the state with the principal number $n$ has $n + 1$ maxima on $r$ axis at the fixed $z$. For the nonzero angular momentum the wave function is zero at $r = 0$ while for $m = 0$ it achieves here the largest maximum. All these properties are in accordance with the general rules of quantum mechanics for the

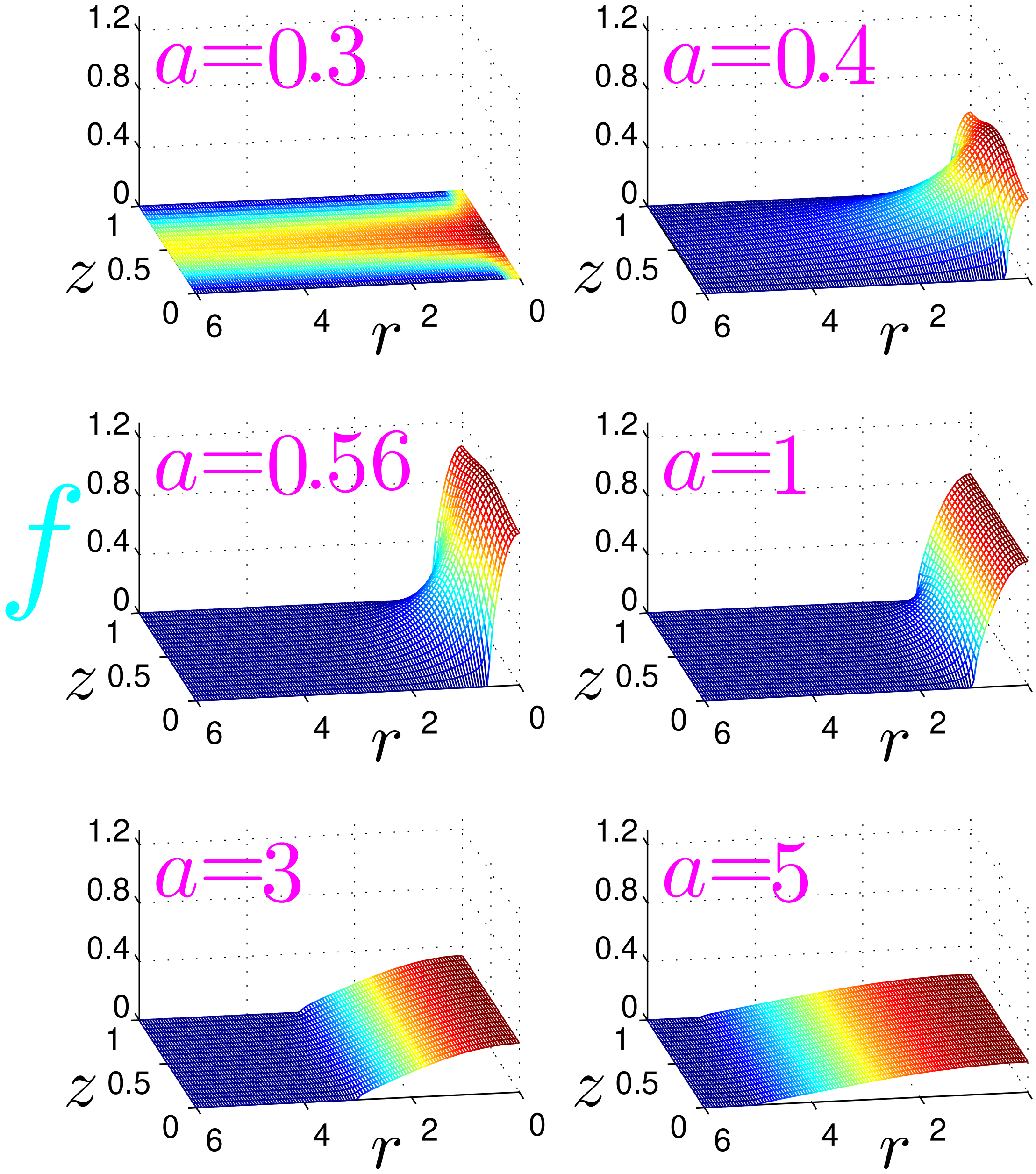


**Figure 4.** The same as in figure 3 but for the two concentric equal Neumann windows on the opposite walls.

radially symmetric systems [42]. Note also that no any radial maxima and minima are observable in the semi infinite DD region: all of them are located in the NN and/or DN part, and the function $f$ exponentially decreases to zero as the radius swipes the $r$ axis to the infinity.

### *4.2. Two different Neumann discs: anticrossings and their evolution*

Next, consider the case of the two concentric Neumann discs with different radii $a$ and $b$ on the opposite walls of the otherwise uniform Dirichlet channel. Only the region

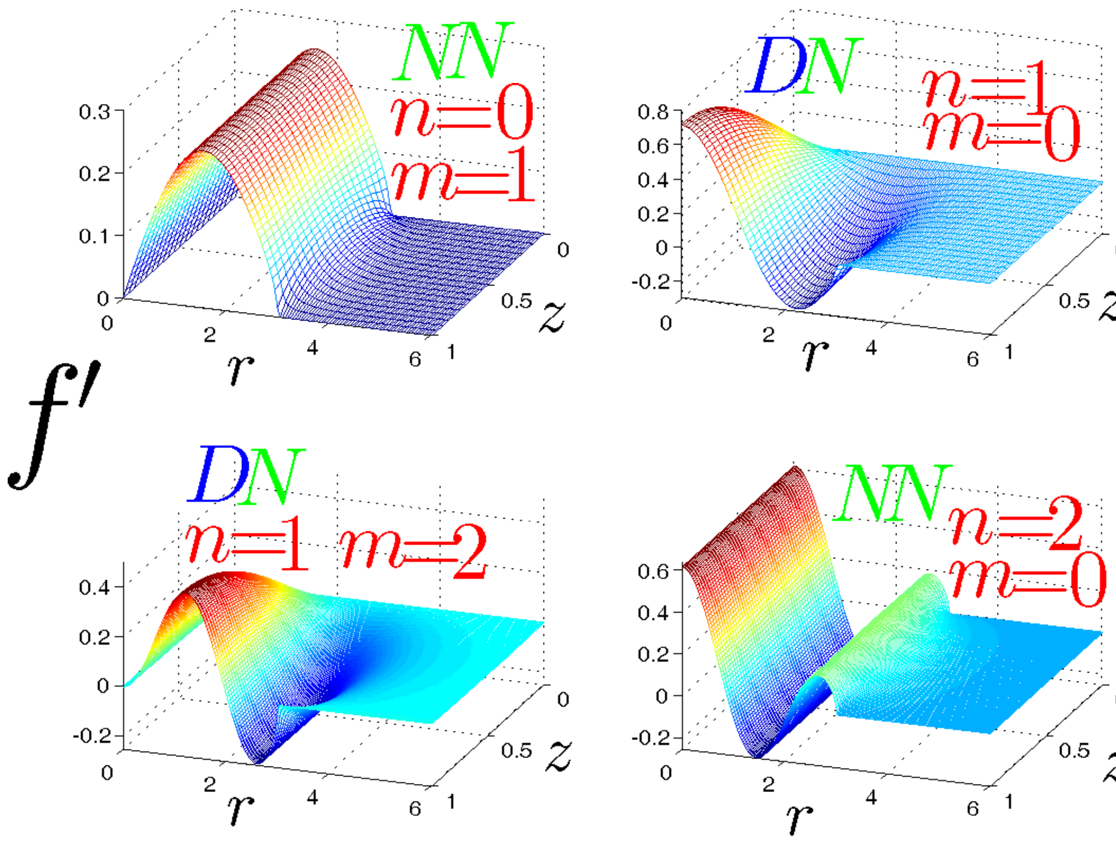


**Figure 5.** Functions $f' \equiv e^{-im\theta} f$ in terms of $z$ and $r$ for the Neumann radius $a = 3$ and several quantum numbers $n$ and $m$. Two capital characters denote a corresponding type of the boundary conditions on the opposite wave guide walls inside the circle $r \leq a$. Note different $f'$-axis scales for each of the panels.

$b/a \leq 1$ is under investigation since, as stated above, we assume that $b \leq a$, $b \geq 0$. Here, one needs to consider three spatial regions: first, for $r \leq b$, when the transverse motion is confined by the two Neumann plates; second, for $b \leq r \leq a$ when the motion in the $z$ direction is governed by the Neumann requirement on the one side and the Dirichlet demand on the opposite walls; and, the last, the region of $r > a$ with the pure Dirichlet transverse boundary conditions. Total solution of (6) for the first region is described by equation (26), for the region of $r \geq a$ it is written as equation (25$b$), and for the ring $b \leq r \leq a$ one has:

$$f(r, \theta, z) = \frac{1}{\sqrt{2\pi}} e^{im\theta} \sum_{j=0}^{\infty} \left[ C_j^{|m|} J_{|m|} \left( \pi \sqrt{E - (j + 1/2)^2} r \right) \right.$$
$$\left. + \; D_j^{|m|} Y_{|m|} \left( \pi \sqrt{E - (j + 1/2)^2} r \right) \right] \chi_j^{ND}(z), \qquad (36)$$

where the Bessel functions $J_{|m|}\left(\pi\sqrt{E - (j+1/2)^2} r\right)$ and $Y_{|m|}\left(\pi\sqrt{E - (j+1/2)^2} r\right)$ for $E < (j + 1/2)^2$ transform into the modified Bessel $I_{|m|}\left(\pi\sqrt{(j+1/2)^2 - E} r\right)$

and MacDonald $K_{|m|}\left(\pi\sqrt{(j+1/2)^2-E}r\right)$ function, respectively, and unknown coefficients $C_j^{|m|}$ and $D_j^{|m|}$ are to be found from the matching of the function $f$ and its radial derivative at the circles $r=b$ and $r=a$. This matching leads again to the eigenvalue equation of the form of (33), where, however, in the present case the infinite matrix $\mathbf{Q}$ takes the block form:

$$\mathbf{Q}=\begin{bmatrix}\mathbf{Q}^{(1)} & \mathbf{Q}^{(2)}\\ \mathbf{Q}^{(3)} & \mathbf{Q}^{(4)}\end{bmatrix}. \tag{37}$$

Here, the infinite matrices $\mathbf{Q}^{(i)}$, $i=1,2,3,4$ have the following elements:

$$\begin{aligned}Q_{jj'}^{(1)}=&\left[\sqrt{\frac{E-(j'+1/2)^2}{E-j^2}}\frac{J'_{|m|}\left(\pi\sqrt{E-(j'+1/2)^2}b\right)}{J'_{|m|}\left(\pi\sqrt{E-j^2}b\right)}\right.\\&\left.-\frac{J_{|m|}\left(\pi\sqrt{E-(j'+1/2)^2}b\right)}{J_{|m|}\left(\pi\sqrt{E-j^2}b\right)}\right]P_{jj'}^{(3)}\end{aligned} \tag{38a}$$

$$\begin{aligned}Q_{jj'}^{(2)}=&\left[\sqrt{\frac{E-(j'+1/2)^2}{E-j^2}}\frac{Y'_{|m|}\left(\pi\sqrt{E-(j'+1/2)^2}b\right)}{J'_{|m|}\left(\pi\sqrt{E-j^2}b\right)}\right.\\&\left.-\frac{Y_{|m|}\left(\pi\sqrt{E-(j'+1/2)^2}b\right)}{J_{|m|}\left(\pi\sqrt{E-j^2}b\right)}\right]P_{jj'}^{(3)}\end{aligned} \tag{38b}$$

$$\begin{aligned}Q_{jj'}^{(3)}=&\left[\sqrt{\frac{E-(j'+1/2)^2}{(j+1)^2-E}}\frac{J'_{|m|}\left(\pi\sqrt{E-(j'+1/2)^2}a\right)}{K'_{|m|}\left(\pi\sqrt{(j+1)^2-E}a\right)}\right.\\&\left.-\frac{J_{|m|}\left(\pi\sqrt{E-(j'+1/2)^2}a\right)}{K_{|m|}\left(\pi\sqrt{(j+1)^2-E}a\right)}\right]P_{jj'}^{(1)}\end{aligned} \tag{38c}$$

$$\begin{aligned}Q_{jj'}^{(4)}=&\left[\sqrt{\frac{E-(j'+1/2)^2}{(j+1)^2-E}}\frac{Y'_{|m|}\left(\pi\sqrt{E-(j'+1/2)^2}a\right)}{K'_{|m|}\left(\pi\sqrt{(j+1)^2-E}a\right)}\right.\\&\left.-\frac{Y_{|m|}\left(\pi\sqrt{E-(j'+1/2)^2}a\right)}{K_{|m|}\left(\pi\sqrt{(j+1)^2-E}a\right)}\right]P_{jj'}^{(1)}.\end{aligned} \tag{38d}$$

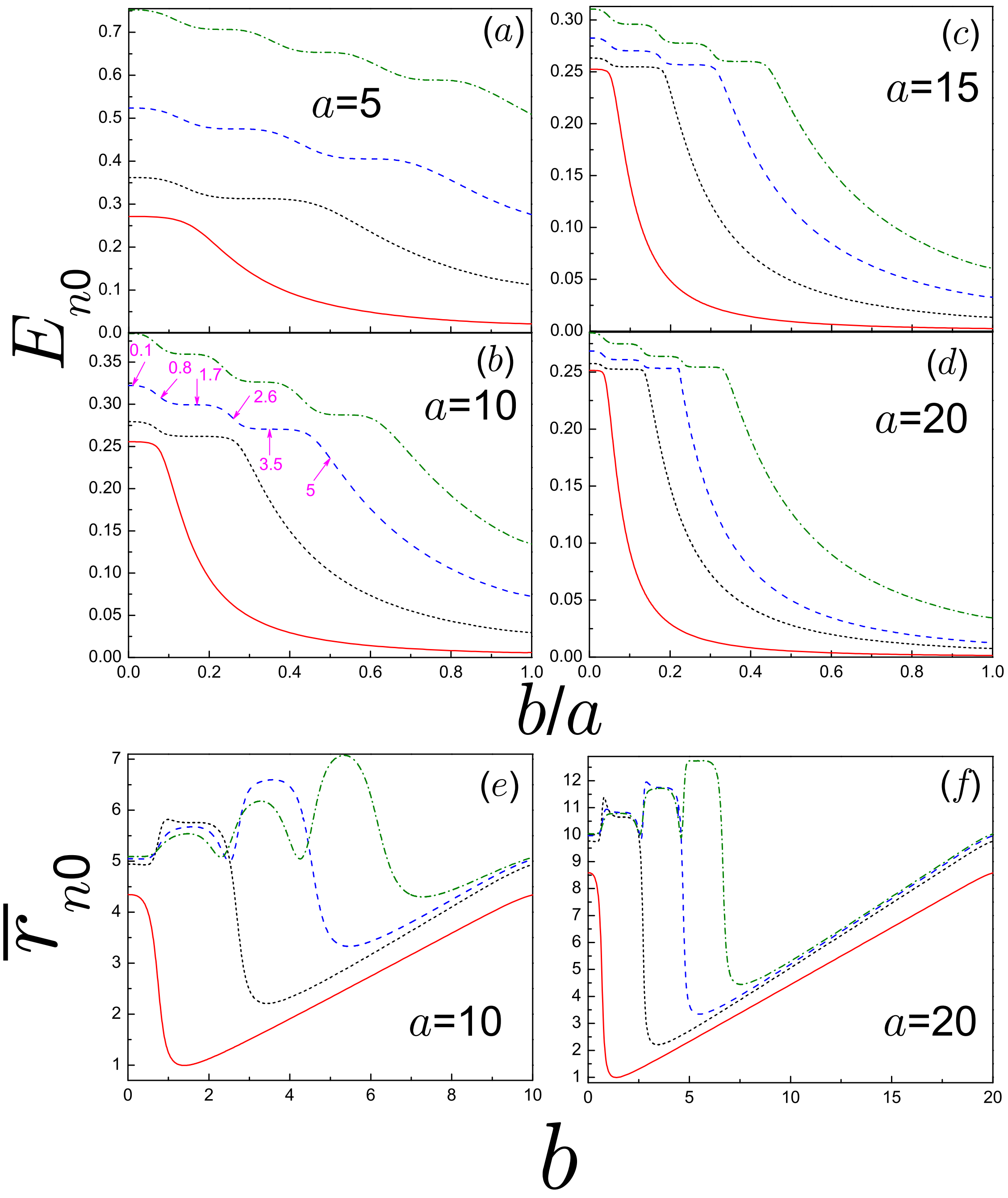


**Figure 6.** (a)-(d) Energies $E_{n0}$ as functions of the ratio $b/a$ for several values of the outer radius $a$ where the panel (a) is for $a = 5$, (b) - for $a = 10$, (c) - for $a = 15$, and (d) - for $a = 20$. Solid lines denote the ground state ($n = 0$), dotted lines depict the energies of the first excited level ($n = 1$), dashed lines are for $n = 2$, and dash-dotted lines - for $n = 3$. Note different energy scales for each of the figures. Arrows in panel (b) show energies for which the corresponding functions $f$ are plotted in figure 7. Numbers near the arrows denote corresponding inner radius $b$. Panels (e) and (f) depict the mean radius $\overline{\rho}_{n0}$ as a function of the inner radius $b$ for $a = 10$ [panel (e)] and $a = 20$ [panel (f)]. The same convention as in panels (a)-(d) is used. Different $\overline{r}$ and $b$ scales are used in each of the panels.

The matrix $\mathbf{P}^{(3)}$ describes the coupling between the pure Neumann transverse motion and its Neumann-Dirichlet counterpart:

$$P_{jj'}^{(3)} = \int_0^1 \chi_j^{ND}(z)\chi_{j'}^{NN}(z)dz$$
$$= \begin{cases} (-1)^{j+j'}\frac{2}{\pi}\frac{j'+1/2}{(j'+1/2)^2-j^2}, & j \neq 0 \\ (-1)^{j'}\frac{\sqrt{2}}{\pi}\frac{1}{j'+1/2}, & j = 0. \end{cases} \tag{39}$$

Energies $E_{n0}$ are plotted in panels (a)-(d) of figure 6 as a function of the radii ratio for several fixed outer radius $a$. Similar pictures are obtained for the nonzero azimuthal numbers $m$ too. As expected, for the vanishing inner radius, $b \to 0$, the energies approach those of the one Neumann window case [30] while for the $b \to a$ one recovers the two equal discs geometry discussed in the previous subsection. Note quite large slope $\partial E/\partial(b/a)$ of the lowest curves depicting the case of the large outer radii $a \geq 10$ [panels (b)-(d)]. The point is that here at both limiting parameters of the inner radius the ground-state energy lies very close to the corresponding fundamental threshold: $E_{00}^{ND} = 1/2$ for $b = 0$ and $E_{00}^{NN} = 0$ for $b = a$. Accordingly, a change of the inner radius forces the particle to undergo transitions from the one situation to the other one and, since this energy interval is large compared to the smaller $a$, one observes rather steep energy descent on $b/a$ axis.

Another remarkable feature of the energy spectrum is emergence and evolution of the avoided crossings between the levels with the same azimuthal number $m$ and different principal numbers $n$. A hint of the anticrossing formation is already seen for the moderate outer radius $a = 5$. As this radius increases, the interval between the levels at $b = 0$ diminishes, as it was discussed in the previous subsection and reference [30]. For the moderate inner radius $b$ its change almost does not affect the energies. This is exemplified in panel (b) of figure 6 where the arrows show the energies at which the functions $f$ are plotted in figure 7 for the second excited level, $n = 2$. It is seen that for the $n$th level the energy stays almost constant with $b$ growing until the expanding NN disc absorbs enough of the first maximum to alter the energy $E$. Further growth of $b$ and its subsequent approach to the first radial node drops the energy of the level to its lower counterpart and significantly distorts the NN maximum. For example, for the case of $b = 0.8$ in panel (b) of figure 6 the corresponding part of figure 7 shows the conspicuous alteration of the first extremum with the first node located at $r \sim 2$. As soon as the expanding inner NN part of the wave guide approaches the next extremum of the function $f$, the energy $E_{nm}$ becomes strongly $b$-dependent. The rapid decrease of the energy in this narrow inner radius range is accompanied again by the strong modification of the wave function $f$. For example, it is seen from the comparative analysis of these two figures that for $b \sim 1.7$ the radial node of the function $f$ is close to the boundary between the NN inner disk and neighbouring ND annulus of the width $a-b$. As a result, we observe an almost flat plateau on the $E$-$b$ dependence. As the second extremum of the function $f$ is approached by the expanding NN disc, it gets strongly distorted what is clearly demonstrated by the corresponding panel for $b = 2.6$ of figure 7. This distortion

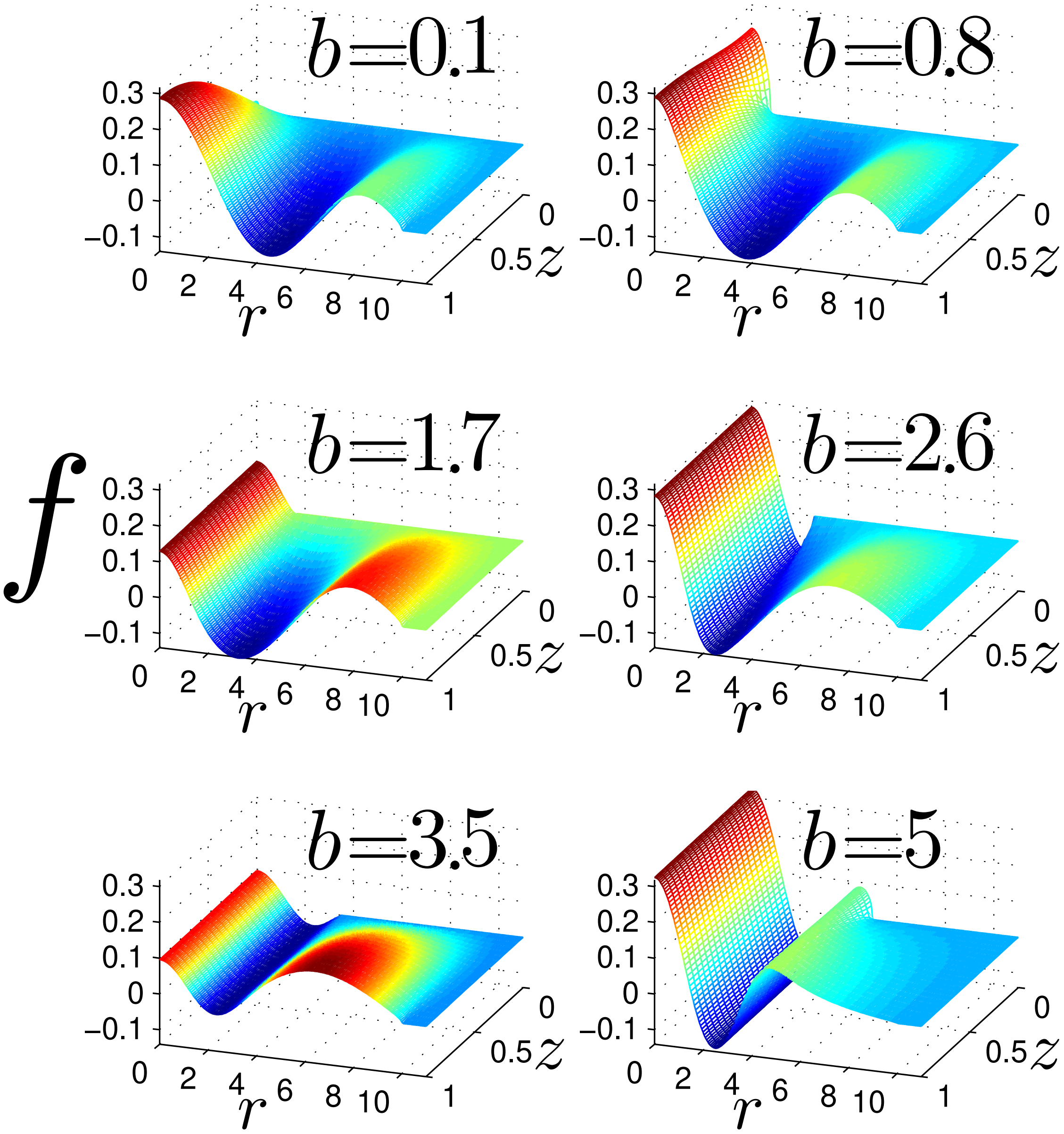


**Figure 7.** Wave function $f_{2,0}$ in terms of $r$ and $z$ for the outer Neumann radius $a = 10$ and several inner radii $b$. Corresponding energies $E_{2,0}$ are shown by the arrows in panel (b) of figure 6.

of the wave function is accompanied by the simultaneous decrease of the corresponding energy $E_{nm}$ until it reaches the plateau of the neighbouring lower lying level with smaller $n$ pushing it downwards. This means that the function extremum fully penetrated into the NN disc; accordingly, the new flat part of the energy spectrum is formed when the boundary between the NN and ND geometries approximately coincides with the node of the function [see arrow for $b = 3.5$ in panel (b) of figure 6 and the corresponding plot in figure 7]. The gap between the $n$th and $(n-1)$th levels at the point of their closest encounter depends on the outer radius decreasing as $a$ increases. The sharpness of the transition between the plateaus increases for the larger outer radius. Such alternating plateau structure with the rapid change between them in the energy spectrum continues until all extrema of the function $f$ are absorbed by the expanding NN disc after which the energy monotonically decreases to its value at $b = a$ [see arrow for $b = 5$ in panel (b) of figure 6 and corresponding function plot in figure 7]. Accordingly, each $n$th level has $(n + 1)$ plateaus. The same structure as the one presented in figures 6 and 7 is observed for the nonzero azimuthal numbers $m$ too where, again, a flat plateau on the $E - b$ dependence corresponds to the NN-ND boundary being located in the vicinity of the node of the function $f$ when the change of the inner radius has a small influence on the eigenvalues of the corresponding Schrödinger equation.

To understand these phenomena better, it is instructive to investigate the mean radius $\overline{r}$ according to

$$\overline{r}_{nm} = \langle\Psi_{nm}|r|\Psi_{nm}\rangle. \tag{40}$$

Its dependence on the inner radius $b$ is shown in panels (e) and (f) of figure 6 for $a = 10$ and $a = 20$, respectively. It is seen that each plateau in the energy spectrum is accompanied by the same flat part of the $\overline{r}$ dependence on the inner radius. Contrary to the energy spectrum, the transition between the plateaus is not smooth; namely, the increasing $b$ at the edge of one plateau initially pushes the wave function closer to the origin, as panels for $b = 0.8$ and $b = 2.6$ demonstrate. This is reflected in the drop of the mean radius. Subsequent growth of the inner radius brings it closer to the next node of the wave function what leads to the formation of the new $\overline{r}$ plateau being located above its predecessor since the function $f$ is distributed wider for the larger inner radius. The sharp drop of the mean radius after the last flat part is explained again by the accumulation of the wave function near the origin (see panel for $b = 5$ in figure 7). After this pronounced minimum the magnitude of $\overline{r}$ smoothly approaches its value of the two equal disc geometry which, quite naturally, coincides with the mean radius of the system with one Neumann window:

$$\overline{r}\big|_{b=0} = \overline{r}\big|_{b=a}. \tag{41}$$

Similar to the energy, the transition between the $\overline{r}$ plateaus gets sharper for the larger outer radii, as the comparison of panels (e) and (f) of figure 6 demonstrates.

Anticrossings very similar to the ones discussed above were calculated for the magnetic quantum ring [43] when the increasing inner radius of the field-free annulus in the otherwise uniform magnetic field for the large fixed values of its outer counterpart forms the avoided crossings of the energies of the adjacent states with the same azimuthal quantum number $m$. Passage through the energy anticrossing in this case is accompanied by the abrupt change of the corresponding whirling persistent current of the same quantum mechanical state what draws the very clear parallel to our geometry with the rapid variations of the mean radius $\overline{r}$. This similarity becomes almost complete if one recalls that the azimuthal current in the uniform magnetic field is determined by the expression from the right-hand side of equation (40) [43]. Energy anticrossings present an ubiquitous feature of the energy spectrum of the quantum systems with finite height potentials [44–58] and are indispensable, for example, in the description of the quantum Hall effect [53].

Finally, we provide the proof of Proposition 3.3. For the large radius, the $z$ dependence of the total function $f(r,\theta,z)$ is defined by $\chi_j^{DD}(z)$, equation (27$a$). In turn, general solution of the radial equation (8) for $E=1$ and $j=0$ is given as

$$R(r)=\left\{\begin{array}{cc} C_1+C_2\ln r, & m=0\\ C_1r^{-|m|}+C_2r^{|m|}, & m\neq 0\end{array}\right. \tag{42}$$

with constants $C_1$ and $C_2$. From the demand of the vanishing of the function $f$ at infinity it immediately follows that $C_2\equiv 0$. In this way, the first term of the right-hand side of equation (24) is obtained. Remaining two terms there can be derived from (25$b$) for $j=1$ and $j\geq 2$, respectively, and asymptotic properties of the Bessel functions $K_{|m|}(x)$ for the large arguments $x$ [37, 38].

## 5. Conclusions

Our comparative analysis has confirmed that the two-Neumann-disc geometry of the otherwise uniform straight 3D Dirichlet wave guide, similar to its one-window counterpart, binds the Schrödinger particle with its energy lying below the essential Dirichlet spectrum. In the former case the binding is stronger than in the latter configuration since the two discs present a larger perturbation to the particle motion in the channel what results in the smaller critical values of the discs radius at which a new bound state emerges from the continuum. Moreover, the change of the second disc diameter opens up an additional channel of manipulating of the spectral and localization properties of the structure and leads to new phenomena such as anticrossings in the energy-inner radius dependence. We have also drawn parallels to the 2D geometry and have revealed a drastic difference between the two cases; namely, if, for the quasi-one-dimensional situation, the state at the critical length with its energy equal to the Dirichlet fundamental propagation threshold is *always* a resonance with non vanishing at infinity wave function, in three dimensions this is true for the states with zero azimuthal quantum number, $m=0$. We have classified the state with $|m|=1$ as a resonance too since its function, even though vanishing at infinity, can not guarantee square integrability while for the larger $|m|$ one has true bound levels with square integrable function.

In our treatment we assumed that the transverse potential is flat. Applying the external electric field $\boldsymbol{\mathcal{E}}$ perpendicular to the interfaces will turn it into the linear tilted one. Influence of the transverse gate voltage $U=\mathcal{E}/d$ on the electronic and optical properties of the pure Dirichlet quantum well has been the subject of intensive theoretical [59–64] and experimental [63] research. It was shown that the field $\boldsymbol{\mathcal{E}}$ significantly changes charged particle behaviour in these low-dimensional nanostructures leading, for example, to the quantum-confined Stark effect [63]. One can expect that for our geometry, similar to the curved 2D Dirichlet wave guides [65], the perpendicular electric field will have a noticeable influence on the bound states too. Such calculations are now in progress.

## 6. Acknowledgements

H.N. acknowledges support from Research Unity 01/UR/15-01. O.O. acknowledges the warm hospitality of Départemente de Mathématiques, ISMAI, Kairouan, Tunisia, where this project was initiated. Research at Jackson State University was financially supported in part by NSF under Grant No. DMR-0606509 and by DoD under contract No. W912HZ-06-C-0057. Stimulating discussions with Prof. P. Exner are gratefully appreciated.

## References

[1] Borisov D I and Gadyl'shin R R 1999 *Teor. Mat. Fiz.* **118** 347
Borisov D I and Gadyl'shin R R 1999 *Theor. Math. Phys.* **118** 272 (Engl. Transl.)
[2] Borisov D I 2001 *C. R. Acad. Sci. Paris Ser. II* **329** 717
[3] Seeley R 2002 *Commun. Part. Differ. Equations* **24** 2403
[4] Driscoll T A and Gottlieb H P W 2003 *Phys. Rev. E* **68** 016702
[5] Borisov D I 2003 *Asymptotic Analysis* **35** 1
[6] Borisov D I 2003 *Izv. RAN Ser. Mat.* **67**(6) 23
Borisov D I 2003 *Izv. Math.* **67** 1101 (Engl. Transl.)
[7] Levitin M, Parnovski L and Polterovich I 2006 *J. Phys. A: Math. Gen.* **39** 2073
[8] Jakobson D, Levitin M, Nadirashvili N and Polterovich I 2006 *J. Comp. Appl. Math.* **194** 141
[9] Zaremba S 1910 *Bull. Intern. Acad. Sci. Cracovie* 314
Zaremba S 1927 *J. Math. Pure Appl. 9 Sér.* **6** 127
[10] Exner P, Šeba P, Tater M and Vaněk D 1996 *J. Math. Phys.* **37** 4867
[11] Exner P and Vugalter S A 1996 *Annales Inst. Henri Poincaré A* **65** 109
[12] Bulla W, Gesztezy F, Renger W and Simon B 1997 *Proc. Am. Math. Soc.* **125** 1487
[13] Davies E B and Parnovski L 1998 *Quart. J. Mech. Appl. Math.* **51** 477
[14] Dittrich J and Kříž J 2002 *J. Math. Phys.* **43** 3892
[15] Borisov D I 2002 *Mat. Sbornik* **193**(7) 37
Borisov D I 2002 *Sb. Math.* **193** 977 (Engl. Transl.)
[16] Dittrich J and Kříž J 2002 *J. Phys. A: Math. Gen.* **35** L269
[17] Borisov D, Exner P and Gadyl'shin R 2002 *J. Math. Phys.* **43** 6265
[18] Olendski O and Mikhailovska L 2003 *Phys. Rev. E* **67** 056625
[19] Borisov D and Exner P 2004 *J. Phys. A: Math. Gen.* **37** 3411
[20] Borisov D I 2004 *Sib. Mat. Zh.* **45** 272
Borisov D I 2004 *Sib. Math. J.* **45** 222 (Engl. Transl.)
[21] Krejčiřík D and Kříž J 2005 *Publ. Res. Inst. Math. Sci.* **41** 757
[22] Borisov D I 2006 *Zh. Vych. Mat. Mat. Fiz.* **46** 284
Borisov D I 2006 *Comp. Math. Math. Phys.* **46** 271 (Engl. Transl.)
[23] Johnson E R, Levitin M and Parnovski L 2006 *SIAM J. Math. Anal.* **37** 1465
[24] Popov I Y and Tesovskaya E S 2006 *Teor. Mat. Fiz.* **146** 429
Popov I Y and Tesovskaya E S 2006 *Theor. Math. Phys.* **146** 361 (Engl. Transl.)
[25] Olendski O and Mikhailovska L 2007 *J. Phys. A: Math. Gen.* **40** 4609
[26] Gortinskaya L V, Popov I Y, Tesovskaya E S and Uzdin V M 2007 *Physica E* **36** 12
[27] Olendski O and Mikhailovska L 2008 *Phys. Rev. B* **77** 174405
[28] Trifanova E S 2009 *Pis'ma Zh. Tekh. Fiz.* **35**(4) 60

Trifanova E S 2009 *Tech. Phys. Lett.* **35** 180 (Engl. Transl.)
[29] Borisov D and Cardone G 2009 *J. Phys. A: Math. Theor.* **42** 365205
[30] Najar H, Ben Hariz S and Ben Salah M 2010 *Math. Phys. Anal. Geom.* **13** 19
[31] Borisov D, Bunoiu R and Cardone G 2010 *Preprint* arXiv:1010.2072v1[math.SP]
[32] Assel R and Ben Salah M *unpublished*
[33] Exner P and Seba P 1989 *J. Math. Phys.* **30** 2574
[34] Schult R L, Ravenhall D G and Wyld H W 1989 *Phys. Rev. B* **39** 5476
[35] Carini J P, Londergan J T, Mullen K and Murdock D P 1992 *Phys. Rev. B* **46** 15538
Carini J P, Londergan J T, Mullen K and Murdock D P 1993 *Phys. Rev. B* **48** 4503
[36] Reed M and Simon B 1978 *Methods of Modern Mathematical Physics* vol IV: Analysis of Operators (New York: Academic)
[37] Abramowitz M and Stegun I A 1964 *Handbook of Mathematical Functions* (New York: Dover)
[38] Watson G N 1966 *A Treatise On The Theory of Bessel Functions* (Cambridge: University Press)
[39] Sprung D W L, Wu H and Martorell J 1992 *J. Appl. Phys.* **71** 515
[40] Gradshteyn I S and Ryzhik I M 2000 *Table of Integrals, Series, and Products* (New York: Academic)
[41] Prudnikov A P, Brychkov Y A and Marichev O I 1986 *Integrals and Series* vol 2 (New York: Gordon and Breach)
[42] Landau L D and Lifshitz E M 1977 *Quantum Mechanics (Non-Relativistic Theory)* (New York: Pergamon)
[43] Kim C S and Olendski O 1996 *Phys. Rev. B* **53** 12917
Olendski O and Kim C S 1997 *J. Korean Phys. Soc.* **31** S461
[44] Maier C H, Cederbaum L S and Domcke W 1980 *J. Phys. B: At. Mol. Phys.* **13** L119
[45] Johnson E A, MacKinnon A and Goebel C J 1987 *J. Phys. C: Solid State Phys.* **20** L521
MacKinnon A and Johnson E A 1988 *J. Phys. C: Solid State Phys.* **21** 3091
[46] Ancilotto F, Selloni A, Xu L. F and Tosatti E 1989 *Phys. Rev. B* **39** 8322
[47] Schulz P A and Tejedor C 1989 *Phys. Rev. B* **39** 11187
Platero G, Brey L and Tejedor C 1990 *Phys. Rev. B* **40** 8548
[48] Fal'ko V I 1992 *Phys. Rev. B* **46** 4320
Fal'ko V I 1993 *J. Phys.: Condens. Matter* **5** 8725
Fal'ko V I 1993 *Phys. Rev. Lett.* **71** 141
[49] Cruz H, Piazza F and Pavesi L 1993 *Semicond. Sci. Technol.* **8** 254
[50] Olendskii O 1993 *J. Phys.: Condens. Matter* **5** 5437
Olendski O 1995 *J. Phys.: Condens. Matter* **7** 5067
Kim C S and Olendski O 1996 *Appl. Phys. Lett.* **69** 2575
Kim C S and Olendski O 1997 *Semicond. Sci. Technol.* **12** 788
[51] Ferreyra J M and Proetto C R 1994 *J. Phys.: Condens. Matter* **6** 6623
[52] Lyo S K 1994 *Phys. Rev. B* **50** 4965
Simmons J A, Lyo S K, Harff N E and Klem J F 1994 *Phys. Rev. Lett.* **73** 2256
[53] Ho T-L 1994 *Phys. Rev. B* **50** 4524
[54] Hagedorn G A and Meller B 2000 *J. Math. Phys.* **41** 103
[55] Exner P and Němcová 2003 *J. Phys. A: Math. Gen.* **36** 10173
[56] Olendski O and Shahbazyan T 2006 *J. Phys.: Conf. Series* **38** 224
Olendski O, Williams Q L and Shahbazyan T 2008 *Phys. Rev. B* **77** 125338
[57] Arsoski V, Tadić M and Peeters F M 2010 *Acta Phys. Polonica A* **117** 733
Tadić M, Arsoski V, Čukarić N and Peeters F M 2010 *Acta Phys. Polonica A* **117** 974
[58] Szafran B and Poniedziałek M R 2010 *Phys. Rev. B* **82** 075320
Poniedziałek M R and Szafran B 2010 *J. Phys.: Condens. Matter* **22** 465801
[59] Rabinovitch A and Zak J 1971 *Phys. Rev. B* **4** 2358
[60] Lukes T, Ringwood G A and Suprapto B 1976 *Physica A* **84** 421
[61] Bastard G, Mendez E E, Chang L L and Esaki L 1983 *Phys. Rev. B* **28** 3241

[62] Nguyen D and Odagaki T 1987 *Am. J. Phys.* **55** 466

[63] Miller D A B, Chemla D S, Damen T C, Gossard A C, Weigmann W, Wood T H and Burrus C A 1984 *Phys. Rev. Lett.* **53** 2173
Miller D A B, Chemla D S, Damen T C, Gossard A C, Weigmann W, Wood T H and Burrus C A 1985 *Phys. Rev. B* **32** 1043

[64] Miller D A B, Chemla D S and Schmitt-Rink S 1986 *Phys. Rev. B* **33** 6976

[65] Exner P 1995 *J. Phys. A: Math. Gen.* **28** 5323